Earth and Planetary Science Letters 295 (2010) 195–204

Contents lists available at ScienceDirect

Earth and Planetary Science Letters

journal homepage: www.elsevier.com/locate/epsl

A model of degassing for Stromboli volcano

A. Aiuppa [a,b,*], A. Bertagnini [c], N. Métrich [c,d], R. Moretti [e], A. Di Muro [f], M. Liuzzo [b], G. Tamburello [a]

[a] CFTA, Università di Palermo, Italy
[b] INGV, Sezione di Palermo, Italy
[c] INGV, Sezione di Pisa, Italy
[d] LPS, CEA-CNRS, Saclay, France
[e] INGV, Sezione di Napoli, Osservatorio Vesuviano, Italy
[f] IPGP/UPMR, Paris, France

ARTICLE INFO

Article history:
Received 8 January 2010
Received in revised form 29 March 2010
Accepted 30 March 2010
Available online 7 May 2010

Editor: R.W. Carlson

Keywords:
volcanic degassing
Stromboli
volcanic gases
CO_2 fluxing

ABSTRACT

A better understanding of degassing processes at open-vent basaltic volcanoes requires collection of new datasets of H_2O–CO_2–SO_2 volcanic gas plume compositions, which acquisition has long been hampered by technical limitations. Here, we use the MultiGAS technique to provide the best-documented record of gas plume discharges from Stromboli volcano to date. We show that Stromboli's gases are dominated by H_2O (48–98 mol%; mean, 80%), and by CO_2 (2–50 mol%; mean, 17%) and SO_2 (0.2–14 mol%; mean, 3%). The significant temporal variability in our dataset reflects the dynamic nature of degassing process during Strombolian activity; which we explore by interpreting our gas measurements in tandem with the melt inclusion record of pre-eruptive dissolved volatile abundances, and with the results of an equilibrium saturation model. Comparison between natural (volcanic gas and melt inclusion) and modelled compositions is used to propose a degassing mechanism for Stromboli volcano, which suggests surface gas discharges are mixtures of CO_2-rich gas bubbles supplied from the deep (>4 km) plumbing system, and gases released from degassing of dissolved volatiles in the magma filling the upper conduits. The proposed mixing mechanism offers a viable and general model to account for composition of gas discharges at all volcanoes for which petrologic evidence of CO_2 fluxing exists. A combined volcanic gas-melt inclusion-modelling approach, as used in this paper, provides key constraints on degassing processes, and should thus be pursued further.

© 2010 Elsevier B.V. All rights reserved.

1. Introduction

The processes driving the endless degassing activity of open-conduit basaltic volcanoes have attracted the attention of volcanologists for decades, and have extensively been studied in recent times thanks to the advent of more and more sophisticated observation techniques. One of the most important though often overlooked aspects of basaltic volcanism is its exceptional gas productivity. The so-called "excess degassing" (Shinohara, 2008), the fact that basaltic volcanoes no doubt emit more gas than potentially contributed by erupted magma, implies an effective gas bubble-melt separation at some point during the ascent. However, while it is universally accepted that separate gas transfer exerts a key control on both quiescent (Burton et al., 2007a) and eruptive (Edmonds and Gerlach, 2007) degassing of basaltic volcanoes, the mechanisms (structural vs. fluid-dynamic control) and depths (shallow vs. deep) of such gas separation are still not entirely understood (Edmonds, 2008).

Volcanic gas investigations have long been hampered by measurement of the most abundant volcanic volatile, water vapour (H_2O): because of the large H_2O concentrations in the background atmosphere, volcanic H_2O detection using FTIR and solar occultation is currently impossible, thus demanding either active (Burton et al., 2000) or passive (using the magma as the source of radiation; Allard et al., 2004) measurements. These limitations have long precluded the acquisition of robust and systematic volcanic gas datasets at open-vent volcanoes, thus making degassing processes easier to probe by studying volatile contents in silicate melt inclusions (MIs) (Blundy and Cashman, 2008; Métrich and Wallace, 2008). Recently, however, the MultiGAS technique (Shinohara et al., 2008) has been established as a cheap and powerful tool for in-situ simultaneous sensing of the three major volcanogenic components (H_2O, CO_2 and SO_2) in volcanic gas plumes (Aiuppa et al., 2007). This, combined with recent developments in H_2O–CO_2 micro-analysis in silicate materials and the refinement of thermodynamic saturation codes, now opens the way to more detailed inspection of degassing processes.

Here, we report on the first MultiGAS measurements including H_2O of the volcanic gas plume of Stromboli, an active basaltic volcano in Southern Italy (Fig. 1). Stromboli, world-known for its mild and uninterrupted Strombolian activity (Rosi et al., 2000), is an ideal

* Corresponding author. CFTA, Università di Palermo, Italy. Tel.: +39 091 23861624; fax: +39 091 6168376.
E-mail address: aiuppa@unipa.it (A. Aiuppa).

0012-821X/$ – see front matter © 2010 Elsevier B.V. All rights reserved.
doi:10.1016/j.epsl.2010.03.040

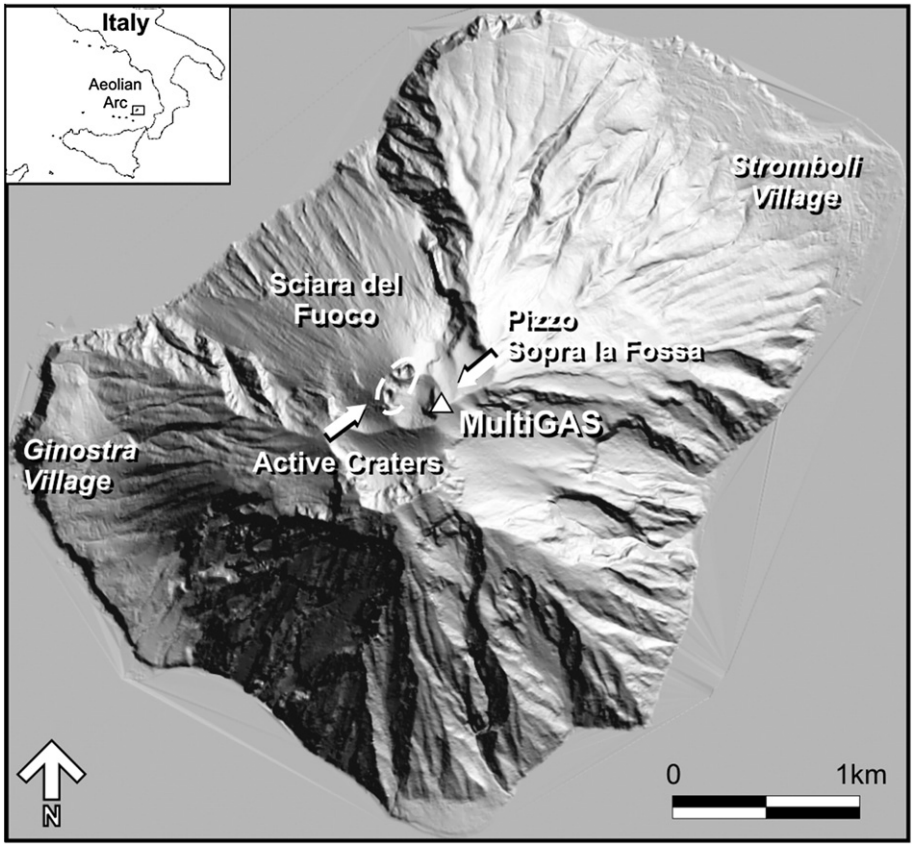

Fig. 1. A map of Stromboli showing the location of the permanent MultiGAS on Pizzo Sopra la Fossa.

target for the modelling of degassing processes, since (i) the persistent open-vent gas emissions are relatively easy to measure (Allard et al., 2008), (ii) the mechanisms driving the persistent Strombolian activity of the volcano and the related seismicity are well characterised (Ripepe et al., 2008), (iii) the petrology of the magmas is intensively studied (Bertagnini et al., 2008), and (iv) clear experimental evidence exists for an efficient gas-melt separation in the plumbing system (Burton et al., 2007b). In spite of this existing knowledge, the structure of the deep and shallow plumbing system is still a matter of debate (Métrich et al., 2010; Pichavant et al., 2009), and information of volcanic gas compositions is still fragmentary, particularly for H_2O. In the attempt to provide a comprehensive model of degassing, we integrate here our volcanic gas observations with recent determinations of volatile contents in melt inclusions (Métrich et al., 2010); and we compare the natural (volcanic gas and MI) data with results from the Moretti and Papale (2004) equilibrium saturation model, which we use to numerically reproduce the degassing trends of Stromboli's magmas upon their ascent and decompression. This combined volcanic gas-melt inclusion-thermodynamic approach finally leads to thorough characterization of degassing processes at Stromboli volcano, with general implications for all basaltic volcanism. Our focus is on the routine Strombolian activity, making our study complementary to recent work (Métrich et al., 2010; Allard, 2010) on the genetic mechanisms of the Stromboli's large scale explosions.

2. Stromboli volcano

The persistent Strombolian activity, for which the volcano is famous, began after the 3rd–7th centuries AD, and since then has continued without significant breaks or variations (Rosi et al., 2000). The current activity takes place at three main craters located in a NE–SW elongated area (the crater terrace) at about 750 m a.s.l. within the Sciara del Fuoco, a deep horse-shoe depression resulting from several lateral collapses (Fig. 1). A variable number of vents (5–15) sustain the typical activity, consisting of intermittent mild explosions lasting few seconds (4–30 s), and with a typical frequency of 13 events/h (Ripepe et al., 2008). The activity is highly variable over timescales of hours and days, and ranges from ash-dominated eruptions to bursts throwing incandescent scoriae and bombs. Emitted products attain heights of a few tens up to hundreds of meters and usually fall in the vicinity of the craters. Explosive activity is associated with a continuous "passive" streaming of gas from the crater area and with active degassing ("puffing") originating from discrete small gas bursts, every 1–2 s.

This routine activity is sporadically interrupted by more energetic explosive events (paroxysms) in which the ejecta fallout reaches the volcano slopes and settled areas along the coast in the largest eruptions. Paroxysms are impulsive events consisting of several explosions from different craters, associated with the ejection of large ballistic blocks and the emission of vertical jets of gas and pyroclasts evolving in short-lived convective columns. A peculiar feature of paroxysms is the co-emission of a nearly aphyric basaltic pumices along with the "usual" crystal-rich scoria (Bertagnini et al., 2003).

Effusive phases also occur on Stromboli, on average every 4 years since 1888. Lava flows are usually related to overflows from the craters or vent opening inside the Sciara del Fuoco. The last effusive episode occurred from 27 February to 2 April 2007, and emitted $\sim 10^7$ m^3 of lava. During the lava effusion, a paroxysmal eruption also occurred (on 15 March), which erupted a significant amount of basaltic pumice (Landi et al., 2009).

During July–December 2008 (the period over which the volcanic gas measurements are reported here), the volcano showed its typical activity, with rhythmic Strombolian explosions of variable energy at

an average frequency of 10–15 events/h (see open-file reports at www.ct.ingv.it). On September 7, December 6 and 17, three slightly more energetic events occurred.

3. Technique

The volcanic gas measurements reported here were carried out from July to December 2008, using the permanent MultiGAS installed on the summit of Stromboli by Istituto Nazionale di Geofisica and Vulcanologia (Sezione di Palermo). This fully-automated instrument has been used for routine measurements of CO_2 and SO_2 concentrations in Stromboli's plume since 2006 (Aiuppa et al., 2009 report on principles of operation, and on CO_2/SO_2 plume ratios in the period from May 2006 to December 2007). In order to measure H_2O, and improve further the quality of CO_2 and SO_2 detection, we used in this study an updated MultiGAS configuration, and more specifically a LI-840 NDIR closed-path spectrometer for both CO_2 (measurement range, 0–3000 ppm; accuracy, ±1.5%) and H_2O (measurement range, 0–80 ppt; accuracy, ±1.5%) (see Shinohara et al., 2008 for details); and a sensitive electrochemical sensor (model 3ST/F, Cod.TD2D-1A, City Technology Ltd., calibration range, 0–30 ppmv; repeatability 1%) for SO_2. Signals from both sensors were captured every 9 s from a data-logger board, which also enabled data logging and storage. After a cycle of 200 measurements, lasting 1800 s in total, a radio link operated automatic data transfer from the remote MultiGAS to the base station in Palermo, where data were elaborated.

Four measurement cycles were operated daily. However, because the instrument is located ~150 m S–SE of the crater terrace (Fig. 1), plume gas sensing was only possible when moderate to strong winds from the northern quadrants blew on the island. In contrast when the plume was gently lofting, rising vertically, or being dispersed north, the MultiGAS consistently detected the typical H_2O (13,000–18,000 ppm), CO_2 (~380 ppm), and SO_2 (<0.1 ppm) concentrations in background air, and the cycle was considered null (e.g., no ratio was calculated from the data). In addition, volcanic H_2O detection was limited to relatively dry and cloud-free conditions on Stromboli's summit (when the plume was not condensing), and in situations when the plume was dense enough for volcanic H_2O to be distinguished from background variations (Fig. 2). In summary, whilst a record of CO_2/SO_2 ratios was achieved on a nearly daily basis, simultaneous detection of the 3 species was only attained 124 times during the record period (Table 1). Accuracy and precision on the

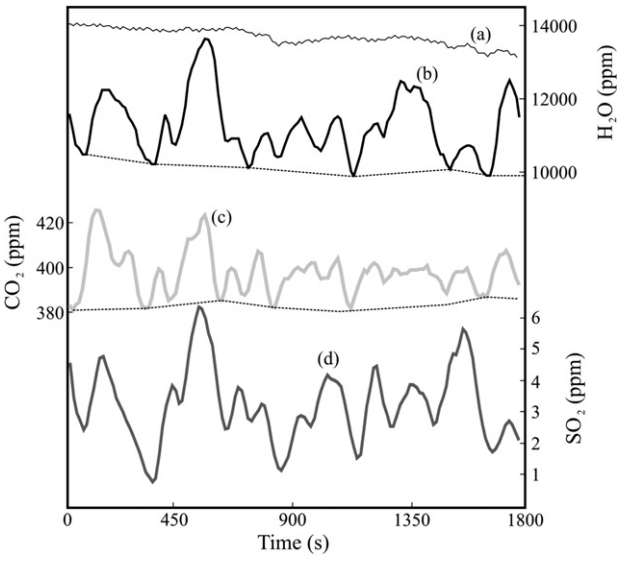

Fig. 2. An example of a 1800 s MultiGAS acquisition at Stromboli (acquisition frequency, 9 s). Whilst small erratic variations of H_2O concentrations are typically measured when the plume is condensing (curve a), more systematic variations (curve b) are observed in dry weather conditions and when the plume fumigates the Pizzo Sopra la Fossa area. These are correlated with variations of CO_2 (curve c) and SO_2 (curve d) concentrations. In such circumstances, volcanic H_2O was derived from the raw data (b) by subtracting background air H_2O content; this required fitting a polynomial function (shown as a dotted line) to H_2O measurements for which a SO_2 content of nearly 0 was consistently detected.

Table 1
Compositions of Stromboli's volcanic gas plume (in mol%). We derive compositions for both the bulk plume (essentially contributed by persistent passive degassing) and the syn-explosive plume (the gas jet of a Strombolian explosion, reaching the MultiGAS a few seconds after the burst, and before being diluted in the main plume).

Date	H_2O	CO_2	SO_2	Date	H_2O	CO_2	SO_2
Bulk plume							
24/7/08	0.91	0.06	0.03	17/9/08	0.81	0.16	0.02
25/7/08	0.91	0.07	0.02	21/9/08	0.56	0.38	0.06
27/7/08	0.95	0.03	0.02	22/9/08	0.93	0.07	0.01
28/7/08	0.89	0.08	0.03	25/9/08	0.72	0.26	0.02
29/7/08	0.94	0.04	0.02	25/9/08	0.78	0.19	0.04
30/7/08	0.95	0.04	0.02	26/9/08	0.56	0.39	0.05
31/7/08	0.97	0.02	0.01	26/9/08	0.82	0.17	0.01
1/8/08	0.97	0.02	0.01	29/9/08	0.59	0.39	0.02
3/8/08	0.97	0.02	0.01	29/9/08	0.79	0.19	0.02
4/8/08	0.83	0.07	0.10	3/10/08	0.48	0.47	0.05
5/8/08	0.97	0.02	0.01	4/10/08	0.75	0.19	0.05
6/8/08	0.81	0.13	0.06	4/10/08	0.96	0.04	0.01
7/8/08	0.87	0.12	0.01	5/10/08	0.70	0.27	0.03
8/8/08	0.97	0.03	0.01	5/10/08	0.80	0.17	0.03
9/8/08	0.98	0.02	0.01	5/10/08	0.82	0.15	0.03
10/8/08	0.85	0.11	0.04	8/10/08	0.89	0.10	0.01
11/8/08	0.97	0.02	0.01	12/10/08	0.93	0.06	0.02
13/8/08	0.98	0.02	0.01	12/10/08	0.95	0.04	0.01
14/8/08	0.96	0.03	0.01	13/10/08	0.89	0.08	0.02
17/8/08	0.91	0.07	0.03	14/10/08	0.90	0.09	0.02
18/8/08	0.94	0.04	0.01	15/10/08	0.83	0.16	0.01
20/8/08	0.72	0.25	0.03	17/10/08	0.77	0.20	0.03
23/8/08	0.98	0.02	0.01	17/10/08	0.86	0.13	0.02
25/8/08	0.98	0.02	0.01	25/10/08	0.75	0.22	0.03
29/8/08	0.90	0.09	0.01	31/10/08	0.79	0.19	0.02
31/8/08	0.86	0.10	0.05	4/11/08	0.80	0.17	0.03
1/9/08	0.95	0.02	0.03	7/11/08	0.83	0.15	0.02
2/9/08	0.96	0.03	0.01	8/11/08	0.68	0.27	0.06
5/9/08	0.93	0.05	0.02	11/11/08	0.55	0.31	0.14
6/9/08	0.95	0.05	0.00	11/11/08	0.80	0.17	0.03
7/9/08	0.78	0.15	0.07	11/11/08	0.54	0.38	0.08
7/9/08	0.96	0.04	0.01	18/11/08	0.89	0.10	0.01
7/9/08	0.91	0.05	0.04	19/11/08	0.91	0.07	0.02
7/9/08	0.97	0.03	0.00	19/11/08	0.77	0.19	0.03
7/9/08	0.88	0.10	0.02	22/11/08	0.90	0.07	0.03
8/9/08	0.73	0.24	0.03	22/11/08	0.65	0.30	0.04
9/9/08	0.89	0.10	0.01	23/11/08	0.49	0.41	0.10
9/9/08	0.86	0.13	0.01	26/11/08	0.78	0.19	0.03
10/9/08	0.75	0.22	0.03	27/11/08	0.64	0.28	0.08
11/9/08	0.93	0.05	0.02	1/12/08	0.71	0.26	0.03
11/9/08	0.74	0.16	0.10	6/12/08	0.54	0.39	0.07
12/9/08	0.64	0.34	0.02	7/12/08	0.72	0.23	0.05
12/9/08	0.91	0.08	0.01	7/12/08	0.65	0.28	0.07
13/9/08	0.95	0.04	0.01	7/12/08	0.90	0.07	0.03
13/9/08	0.97	0.03	0.00	7/12/08	0.60	0.34	0.06
15/9/08	0.90	0.09	0.01	9/12/08	0.63	0.34	0.04
15/9/08	0.77	0.21	0.02	10/12/08	0.58	0.35	0.07
16/9/08	0.81	0.17	0.02	12/12/08	0.59	0.34	0.07
16/9/08	0.88	0.11	0.01	17/12/08	0.78	0.20	0.02
16/9/08	0.60	0.31	0.09	24/12/08	0.80	0.16	0.04
17/9/08	0.89	0.06	0.04	24/12/08	0.85	0.13	0.02
Syn-explosive gas							
27/7/08	0.66	0.31	0.03	4/10/08	0.83	0.16	0.01
2/8/08	0.88	0.12	0.00	6/10/08	0.59	0.39	0.02
7/9/08	0.88	0.11	0.01	12/10/08	0.87	0.12	0.01
13/9/08	0.86	0.14	0.00	14/10/08	0.78	0.21	0.01
15/9/08	0.72	0.27	0.01	15/10/08	0.85	0.15	0.01
15/9/08	0.77	0.23	0.01	27/10/08	0.72	0.28	0.01
16/9/08	0.72	0.25	0.02	11/11/08	0.60	0.36	0.04
17/9/08	0.83	0.16	0.01	19/11/08	0.70	0.27	0.02
17/9/08	0.58	0.41	0.01	4/12/08	0.71	0.28	0.01
23/9/08	0.71	0.28	0.01	7/12/08	0.67	0.31	0.02
29/9/08	0.49	0.50	0.01	12/12/08	0.65	0.34	0.01

sensors was periodically checked (every 2 moths) using standard gas mixtures and a dew point generator (for H_2O).

4. Results

4.1. Raw data and calculation of volcanic gas composition

Fig. 2 shows an example of 1-cycle acquisition from the permanent MultiGAS at Stromboli. When the plume was condensing, H_2O concentrations varied smoothly and randomly during the 1800 s acquisition period (curve a), precluding any retrieval. In contrast, larger variations of H_2O concentrations (curve b) were captured in the optimal conditions (dry weather conditions, plume fumigating the area of Pizzo Sopra la Fossa, see Fig. 1), which were broadly correlated with time variations of CO_2 (curve c) and SO_2 (curve d). In these circumstances, the temporal changes of concentrations reflected variable extents of dilution of volcanic gases in the background atmosphere upon plume dispersal (due to changes in plume travelling speed and direction, or changes in source strength).

From the raw plume concentration data (in ppm), the volcanic gas plume H_2O/SO_2 and H_2O/CO_2 ratios were derived by calculating the gradients of the best-fit regression lines in H_2O vs. SO_2 and H_2O vs. CO_2 scatter plots (Fig. 3), as previously reported for Etna (Shinohara et al., 2008). Then, the (air-free) composition of volcanic gases (in mol%; Table 1) was finally calculated by combing together each suit of gas concentration ratios, and normalizing to 100%. This assumes that contributions from undetected species (e.g., H_2, H_2S, HCl) are relatively minor.

While plume ratios were generally relatively constant within each measurement cycle (e.g., R^2 of best-fit regression lines were normally >0.7, and standard deviations of the derived ratios ≤25%), brief but significant variations of the ratios were sometimes observed (Fig. 4). Visual observations and cross correlations of our dataset with seismic and thermal signals (available at http://www.ct.ingv.it) indicated that such short-term variations (generally lasting less than 2 min) systematically occurred soon after individual Strombolian bursts. We therefore suggest they reflect our measurements capturing of the composition of the syn-explosive gas phase (e.g., the gas jet released during the short-lived Strombolian explosions). When the wind was particularly strong and explosive activity high, this syn-explosive gas phase, known to be compositionally distinct from the quiescent plume (Burton et al., 2007b), eventually reached the instrument (a few seconds after the explosion) before being diluted (and homogenised) within the bulk plume. Our data support further the earlier conclusions of Burton et al. (2007b), demonstrating that the syn-explosive gas phase is significantly richer in CO_2 (and poorer in H_2O and SO_2) than the bulk plume (Fig. 4 and Table 1). The latter is mainly contributed by (quiescent) passive degassing in between the explosions, and by puffing activity at the open vents (Ripepe et al., 2008).

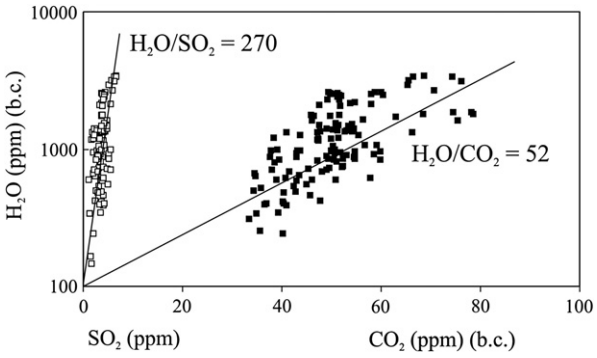

Fig. 3. Scatter diagram of H_2O vs. SO_2 and H_2O vs. CO_2 concentrations acquired during 1 measurement cycle. The H_2O/SO_2 and H_2O/CO_2 plume ratios are calculated from the gradient of the best-fit regression lines.

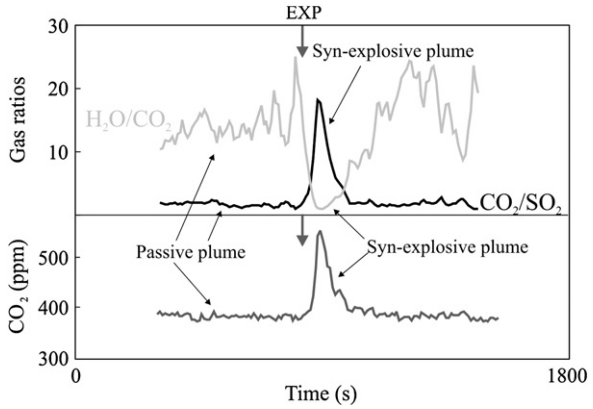

Fig. 4. High-resolution (9 s) record of (a) plume ratios and (b) CO_2 concentrations, showing the contrasting compositions of the passive and syn-explosive gas plume emissions. In the most favourable conditions (strong winds blowing from the N), a Strombolian explosion (grey arrow labelled "EXP") is followed (with a time-lag of a few seconds) by a brief (lasting a few minutes) but significant increase of CO_2 concentrations and CO_2/SO_2 ratios detected by the MultiGAS. The syn-explosive gas phase is typically H_2O-poorer (and CO_2-richer) than the passive plume released in between explosions (this contribution by far dominating Stromboli's bulk plume emissions in the long-term).

4.2. The H_2O–CO_2–SO_2 composition of Stromboli's plume

Ignoring minor components, Stromboli's gas composition is dominated by H_2O (48–98 mol%; mean, 80%), CO_2 (2–50 mol%; mean, 17%) and SO_2 (0.2–14 mol%; mean, 3%) (Table 1). As such, they resemble quite closely the typical composition of volcanic gases from arc-settings, though sharing with nearby Etna (Shinohara et al., 2008) a characteristic of CO_2-enrichment (most volcanic gases from arc basaltic volcanoes have >90% H_2O; Shinohara, 2008).

Stromboli's syn-explosive gas phase is richer in CO_2 (11–50%; mean 26%) and poorer in H_2O (48–88%; mean, 73%) than the bulk plume passively released by the volcano's open vents in between the explosions (mean CO_2 and H_2O, 15 and 82%, respectively) (Table 1). Our measurements of the syn-explosive gas phase are in qualitative agreement with previous determinations (CO_2 19–33%; H_2O 64–79%; Burton et al., 2007b), and thus confirm further the bimodal nature of the emission chemistry at Stromboli.

The most striking feature of the dataset is the large spread of plume compositions observed in only 6 months of observations. This is clearly shown in Fig. 5, where H_2O/CO_2 and CO_2/SO_2 ratios show a distinct antithetic behaviour: the syn-explosive gas phase is characterised by high CO_2/SO_2 ratios (>10, and as high as 47) and low H_2O/CO_2 ratios (<6, but typically between 1 and 3); while the bulk plume is

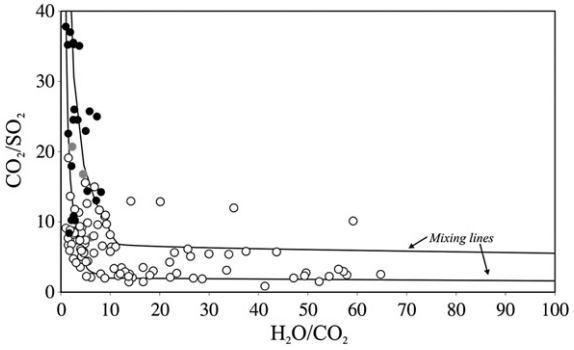

Fig. 5. In a H_2O/CO_2 vs. CO_2/SO_2 scatter plot, Stromboli's plume gas emissions are shown to range from CO_2-rich to H_2O-rich. The syn-explosive (black circles) and quiescent (open circles) plumes have distinct compositions, with some overlap. Grey circles are FTIR-sensed gas compositions for Strombolian explosions (Burton et al., 2007b). Curves labelled "Mixing lines" are calculated as described in the caption of Fig. 8, and in Section 5.2.

generally characterised by lower (<15) CO_2/SO_2 ratios and higher H_2O/CO_2 ratios (1.5–65). Note that virtually all H_2O-rich (H_2O/CO_2 ratios >30) bulk plume compositions have low (<6) CO_2/SO_2 ratios. The same diagram highlights however that syn-explosive and bulk plume compositions are somewhat overlapping, and that the bulk plume can be substantially CO_2-richer (but also more H_2O rich) than previously measured (representative CO_2/SO_2 and H_2O/CO_2 ratios of ~8 and ~6 were previously quoted for the bulk plume, respectively; Burton et al., 2007b). The results are in agreement with the large variation of the bulk plume CO_2/SO_2 ratio (range, 0.9–26) observed in a 19 months period encompassing the recent February–April 2007 effusive eruption of Stromboli (Aiuppa et al., 2009); including the detection of an exceptionally CO_2-rich plume (CO_2/SO_2 up to 26) before the onset of the eruption, and prior to the paroxysm on March 15, 2007.

5. Discussion

The striking range of volcanic gas compositions at Stromboli suggest dynamic magma degassing processes at this open-vent volcano. Indeed, whilst some persistently degassing volcanoes display an apparent stability in both activity state and volcanic gas composition for years (e.g., Nyiragongo, Sawyer et al., 2008), Stromboli shares with nearby Etna (Aiuppa et al., 2007) a time-changing nature of both volcanic activity state and volcanic gas composition.

Remarkable short-period (seconds) variations in volcanic gas compositions at Stromboli were first documented based on high-frequency FTIR measurements (Burton et al., 2007b); these demonstrated that the volcanic gas phase released during the short-lived Strombolian explosions are richer in CO_2 (and poorer in Cl) than the bulk (quiescent) plume. Since CO_2 is significantly less soluble in basaltic melts than H_2O, S, and Cl, and thus deeply exsolved, it was concluded that the gas slugs feeding Strombolian explosions have a relatively deep provenance (0.8–2.7 km below the summit vents). This deep source area also supported the idea of a separate ascent of gas and melt in the shallow (less than 2.7 km) plumbing system, as also proposed for other basaltic systems (Edmonds and Gerlach, 2007). Our measurements here extend further the conclusions of Burton et al. (2007b): the temporal variability of the composition of the bulk (quiescent) plume requires the existence of a complex degassing regime in which a separate gas ascent plays a key role (Pichavant et al., 2009). Visual observations suggest that the bulk Stromboli's plume is essentially contributed by both quiescent (passive) gas release from the magma ponding at the crater terrace' open vents, and by small bursts of over-pressurised gas pockets at the magma-free atmosphere (Harris and Ripepe, 2007). It follows then that the most obvious source for the bulk gas emissions would be degassing of volatiles dissolved in the magma filling the upper conduits, and ultimately the high porphyricity (HP) magma ponding at the open vents, and erupted as scoriae during Strombolian explosions. However, the variable composition of the bulk plume, and its recurrent CO_2-rich signature (see Fig. 5) are not consistent with this hypothesis: the HP magma is volatile-poor (see Sections 5.1 and 5.2 below), and its degassing upon decompression (followed by near-surface gas separation) cannot produce a gas phase with a CO_2/SO_2 ratio greater than ~0.5–1 (see Section 5.3 below), which is substantially lower than observed (Fig. 5).

In order to model the source processes controlling the chemistry of Stromboli's volcanic gases, we combine in the sections below the record of pre-eruptive volatile contents in Stromboli's magma, as derived from MI analysis (Section 5.1), with the results of numerical simulations carried out using the Moretti and Papale (2004) saturation model (Section 5.2). These calculations allow quantitative reproduction of the evolving composition of the gas phase released by Stromboli's magmas upon their storage and ascent within the crust. Finally, comparison between modelled and observed volcanic gas compositions (Section 5.3) offers new clues on volcanic degassing processes, and on the structure of the magmatic plumbing system of Stromboli.

5.1. Melt inclusion record of magma ascent and degassing

There is consensus (Bertagnini et al., 2008) that two magma types are involved in the present-day Stromboli's activity. The emission of nearly aphyric highly vesicular pumice during paroxysmal eruptions highlights the existence of a low porphyritic (LP), volatile-rich HK basalt magma residing in the deep volcano plumbing system (Fig. 6). Dissolved CO_2 and H_2O contents (0.15–0.2 and 2.5–3.5 wt.%, respectively; Fig. 7a) in olivine-hosted basaltic melt inclusions (MIs) were used (Métrich et al., 2010) to show that the LP magma is stored in a 7–10 km deep reservoir (equivalent to 190–260 MPa pressure) (all depths are below the summit vents, bsv). The LP magma is thought to coexist with a substantial (~2 wt.%) fraction of CO_2-rich gas bubbles at reservoir conditions (Burton et al., 2007a,b). Observations on erupted pumices strongly suggest that, prior to a paroxysm, the LP magma is rapidly decompressed, maintaining virtually unchanged his "deep" petrological (Métrich et al., 2010) and textural (Polacci et al., 2009) properties.

The persistent behaviour of the volcano implies that a supply of deeply derived magmas must occur not only prior to/during a paroxysm, but also during the normal Strombolian activity (yet at a slower rate). However, since the LP magma is only erupted during high energy explosive activity, while a volatile-poor shoshonitic basalt (the HP magma) feeds the normal Strombolian activity, a mechanism leading to LP to HP magma transition must "normally" take place somewhere in the plumbing system. According to melt inclusion record (Métrich et al., 2010), ascending LP magmas undertake an extensive water loss in the 2–4 km bsv depth range (equivalent to 50–100 MPa pressure), with H_2O decreasing to <1.5 wt.%. This has three main implications and consequences:

(i) first, de-hydration of a magma can be caused by fluxing with deep-rising CO_2-rich gas (Spilliaert et al., 2006), a fact which is suggestive of the presence of a magma ponding zone at 2–4 km bsv, where CO_2-rich gas bubbles accumulate to contents >5 wt.% (Métrich et al., 2010). An intermediate magma ponding zone at Stromboli is also supported by geodetic data (Bonaccorso et al., 2008);

(ii) secondly, for the magma to become extensively de-hydrated, it is required that gas bubbles escape from this ponding zone, a fact which might be favoured by the presence of a geological discontinuity (the interface between volcanic rocks and the basement lies at about 2.4–3.5 km depth; Di Roberto et al., 2008), and/or promoted by vesicularity of the magma reaching a critical threshold for gas percolation (and permeable gas flow) (Burton et al., 2007a). Whatever the cause, magma de-hydrated thus implies gas-melt separation (and thus transition to open-system degassing regime) at 2–4 km bsv depth;

(iii) finally, de-hydration of the stored magmas raises their liquidus temperatures, hence promoting extensive crystallization (Métrich et al., 2001, 2010; Di Carlo et al., 2006), and ultimately leading to transition from the LP to the H_2O poor (<1.5 wt.%; Fig. 7a) and crystal-rich (30–50%) HP magma (Fig. 6). The highest dissolved volatiles contents in MIs from the plagioclase-bearing HP magma (Fig. 7a) indicate entrapment pressures of ~50–100 MPa pressure (Métrich et al., 2010), confirming that a change from closed- to open-system degassing regime (with the consequent water depletion being the trigger for transition from LP to HP magma) occurs in the 2–4 km bsv depth range.

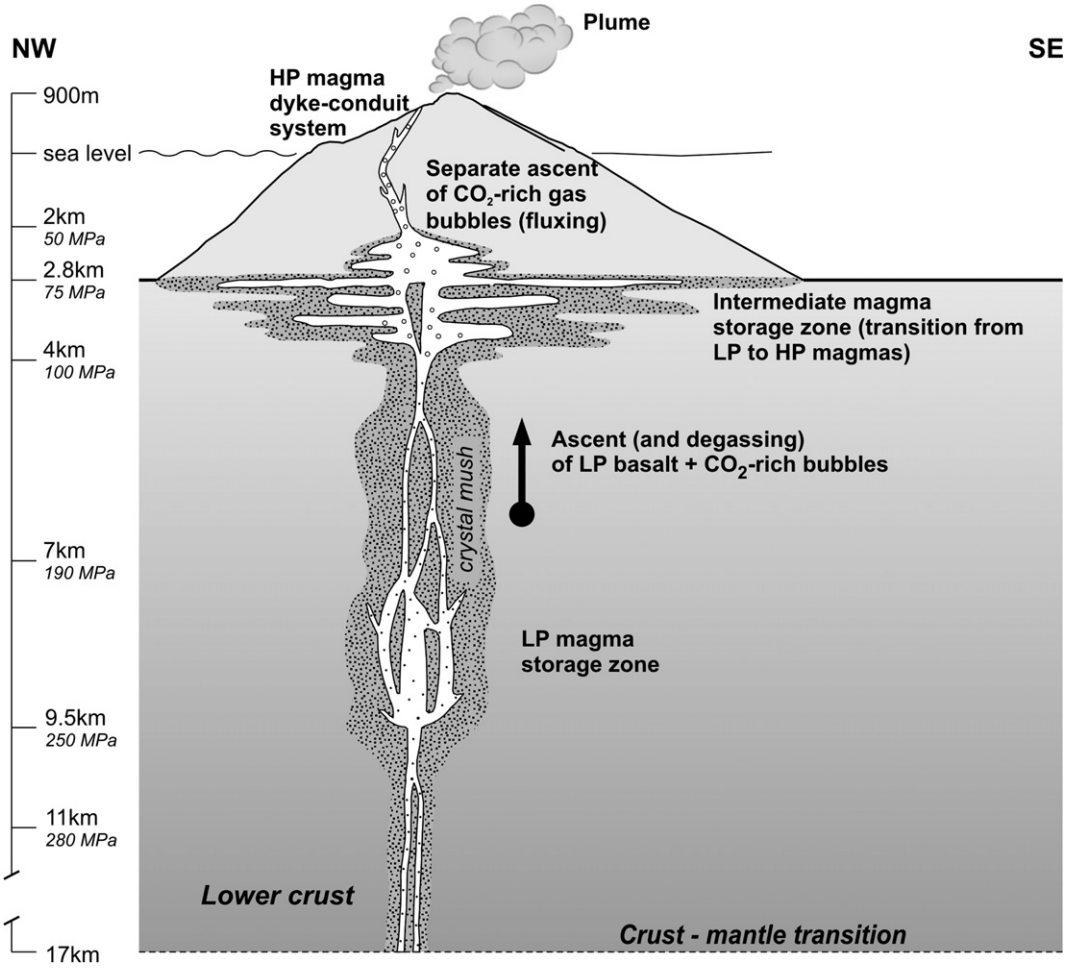

Fig. 6. Schematic cross-section showing the main features of Stromboli's crustal plumbing system (modified from Métrich et al., 2010). See text for discussion.

The contrasting compositions, volatile contents, and depth of storage of LP and HP magmas (Table 2) imply that the magmatic gas phases in equilibrium with (and separated from) these two magma types are inevitably different, as calculated below.

5.2. Numerical modelling

Volatile contents in MIs (Table 2) are used here to initialize model calculations of volatile partitioning between the magmatic gas phase and the melt, which we performed using the code described in Moretti and Papale (2004). This code allows calculating the volatile (C–H–O–S system) equilibrium composition of coexisting magmatic vapour and silicate melt at a given set of pressure and temperature conditions.

In this study, we utilised the code to perform two sets of complementary calculations. In a first set of model runs (hereafter referred as LP runs), we calculated the composition of the magmatic gas phase in equilibrium with Stromboli's LP magma, in a range of pressure conditions representative of the deep plumbing system. LP runs were initialised with the input parameters summarised in Table 2. All LP runs were carried out by stepwise decreasing pressure from an initial value of 300 MPa (the deepest roots of the plumbing system probed by MIs) down to 100 MPa (the entrapment pressure of the most volatile-depleted MIs or glass embayments in LP magmas; Fig. 7a). The model results are critically dependent on the choice of the total (exsolved + dissolved) magma CO_2 content: four sets of LP runs were thus carried out at different CO_2 contents (0.2, 2, 5 or 20%, respectively), to account for the presence of a non-negligible (but poorly constrained) fraction of CO_2-rich gas bubbles at reservoir conditions. While a 2 wt.% CO_2 content is supported by gas budget computations (Allard et al., 2008; Allard, 2010), an even higher (5 wt. %) content is consistent with melt inclusion evidences (Métrich et al., 2010); the run at 20% CO_2 content should only be viewed as an end-member composition calculation (and not an authentic representation of the natural case).

The second set of model runs (referred as HP runs) attempted at calculating the composition of the magmatic gas phase in equilibrium with Stromboli's HP magma. The input parameters of HP runs (Table 2) were adapted to fit at best conditions prevailing in the shallowest part of the plumbing system. The highest entrapment pressure (~100 MPa) derived from volatile contents in MIs (Table 2) was taken as the starting pressure of our simulations, followed by step-wise pressure decrease in first closed-system to then open-system conditions. Transition from closed- to open-system conditions was fixed at 50 MPa (or ~2 km bsv), the pressure at which vesicularity of the HP magma is thought to become high enough for gas percolation through a network of inter-connected bubbles to occur (Burton et al., 2007a). As discussed before (cfr. 5.1), open-system degassing may prevail from even deeper (to as deep as 4 km bsv, or 100 MPa pressure); sensitivity tests made with different (deeper) closed-open transition depths demonstrated however a minor effect on the degassing trends.

5.2.1. Model results, and comparison with natural data

The outputs of model calculations are, for each run and at each pressure, the equilibrium volatile compositions of coexisting melt and vapour phases. These are contrasted against natural (MIs and volcanic gas) data in Figs. 7 and 8, respectively. Our model results are

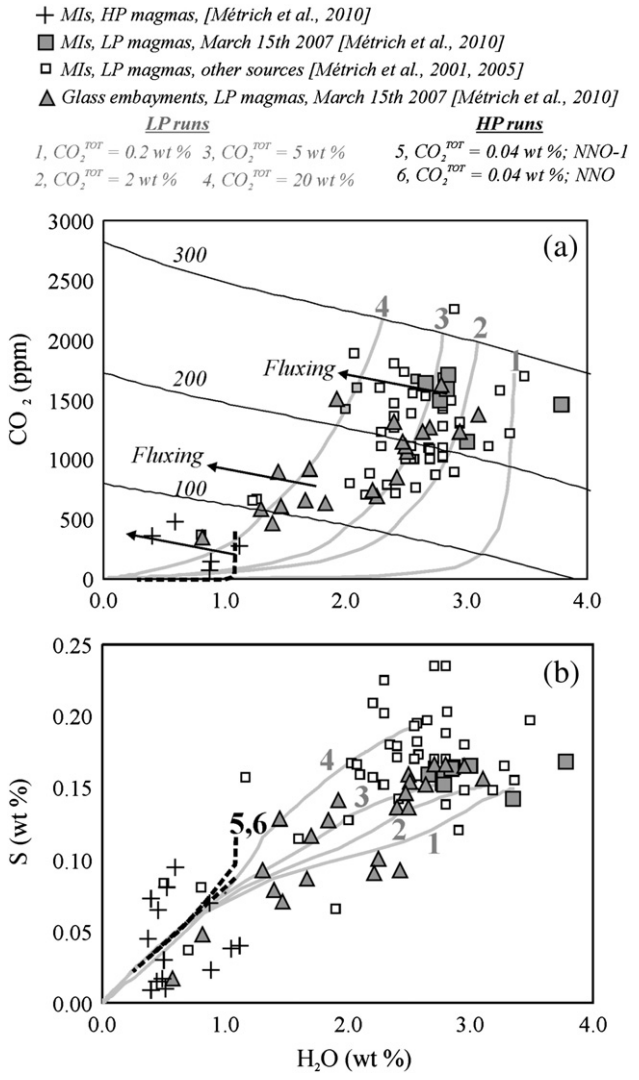

Fig. 7. Volatile abundances in Stromboli's melt inclusions and glass embayments contrasted against results of the saturation model. Data from Métrich et al. (2001, 2005, 2009) and Bertagnini et al. (2003). (a) H_2O vs. CO_2; (b) H_2O vs. S. The grey solid lines are model results from LP runs 1–4, whilst black dashed lines show model results from HP runs 5–6. Comparison of natural and modelled compositions confirms that the deep (P>100 MPa) LP magma contains a high (2–5 wt.%; model curves 2–3) fraction of gas bubbles at reservoir conditions. Glass embayment formed at P~100 MPa are H_2O-poorer than predicted by model curves 2–3, suggesting some extent of gas fluxing with CO_2-rich gas bubbles. This triggers de-hydratation of the LP magma, and probably controls transition to HP magma. The same process likely occurs also in the upper conduit system (compare model trends 5–6 with volatile abundances in HP magmas). In a, isobars are traced under a fixed Fe_2/Fe_{tot} ratio of 0.24 (Table 2), and are thus slightly different than those originally reported by Métrich et al. (2010) (who, yet using the same saturation model, used a constant ΔNNO value, thus yielding variable Fe_2/Fe_3 proportions depending on melt composition, and water particularly).

qualitatively similar to the pressure-related model degassing trends presented by Allard (2010) (see his Fig. 3), which were yet based on the use of different saturation model and assumptions.

Fig. 7a and b reveal a reasonable agreement between modelled dissolved volatile contents in melt and measured H_2O–CO_2–S abundances in MIs and glass embayments. The plots demonstrate that model runs 2–3 are those showing the best fitting with MI data (squares), suggesting that the LP magma may actually coexist at reservoir conditions with a significant (2–5 wt.%) fraction of CO_2-rich gas bubbles (Allard et al., 2008). Glass embayments (triangles) provide a snapshot of the decompression path of the LP magma shortly prior to a paroxysm (Métrich et al., 2010), and are substantially more volatile-depleted than melt inclusions: their H_2O-poor compositions (Fig. 7a), with most samples trapped in the 150–50 MPa pressure range plotting to the left of curves 2–3, support re-equilibration of the melt with an even larger (>5 wt.%) proportions of CO_2-rich gas bubbles. As such, the volatile compositions of glass embayments may reflect gas-melt interactions within the CO_2-rich intermediate (2–4 km deep) magma ponding zone (cfr. 5.1). Finally, we observe that modelled compositions from HP runs are reasonably consistent — though richer in H_2O — with MI record. The apparent H_2O-depletion captured by MIs (relative to model curves) is an hint for that magma fluxing by CO_2-rich gas bubbles (leading to magma de-hydration) has a major impact on magma resident in the upper conduit, as observed elsewhere (Collins et al., 2009). Modelled dissolved sulphur contents (Fig. 7b) are also consistent with MI record, and again support a mechanism of progressive increase of the CO_2^{TOT}/H_2O^{TOT} ratio from trends 1 to 4. We also observe that, at the given redox conditions and CO_2^{TOT} contents, sulphur starts exsolving at high pressure (Fig. 7b), thus accompanying water loss. All degassing H_2O–S trends converge to a common rectilinear path in the H_2O-depleted (<1 wt.%) range.

The fair agreement between modelled and natural compositions, observed in Fig. 7, supports the computational capabilities of the code, and therefore provides confidence of the calculated composition of the magmatic gas phase. Our model results, summarised in Fig. 8, indicate that a CO_2-rich magmatic gas phase coexists with the LP magma over its entire 300–100 MPa decompression path (curves 1–4). At the reservoir pressure of ~210 MPa, the most likely source area for LP magmas erupted on the most recent (15th March 2007) paroxysm (Métrich et al., 2010), the calculated H_2O/CO_2 and CO_2/SO_2 ratios for the modelled magmatic gas are in the range 0.5–0.95 and 176–363, respectively (depending on run conditions). These modelled gas compositions for the LP runs are therefore more CO_2 rich than our measured volcanic gas compositions (Fig. 8). We note however that some of the richest CO_2 volcanic gas data are consistent with model gas compositions calculated at P = 100–120 MPa in the LP model run 1 (CO_2^{TOT} = 0.2 wt.%; Fig. 8).

As for the HP run results, the calculated pressure-dependent evolution of the magmatic gas phase released by decompressing HP magmas is shown in Fig. 8 by curves 5 and 6. The diagram shows an evident shift in calculated gas compositions, from CO_2-rich at high pressure (100 MPa) to H_2O-rich (and CO_2-depleted) at low pressure (0.1 MPa). The latter compositional trends partially overlap the range of measured volcanic gas compositions (Fig. 8).

5.3. A model of degassing for Stromboli volcano

Our model calculations above provide a quantitative background for interpreting the source processes controlling the time-changing composition of Stromboli's volcanic gases. Based on the model results, we propose that two main gas contributions sustain the persistent surface gas discharges of the volcano.

To start with, MI determinations (cfr. 5.1) and gas measurements (Burton et al., 2007a,b, and this study) offer ample evidence for that the shallow Stromboli's plumbing system is fluxed by the ascent of CO_2-rich gas bubbles. This mechanism of CO_2 fluxing is consistent with the mantle to deep-crustal CO_2 exsolution in basaltic systems, and has been unambiguously supported at several volcanic systems by recent textural (Rust et al., 2004), melt inclusion (Johnson et al., 2008), and volcanic gas (Shinohara et al., 2008) studies. At Stromboli, in particular, the separate ascent of CO_2-rich gas bubbles plays a key control on magma de-hydration in the 0–4 km depth range (e.g., for P<100 MPa), and is as such the trigger for the LP to HP magma transition in the intermediate (2–4 km) magma ponding zone (Fig. 6). The composition of the deep-rising CO_2-rich gas bubbles will be dependent on the depth on their separation from (and thus last equilibration with) the silicate melt. In the most extreme conditions,

Table 2
List of input parameters of model runs. LP runs simulate isothermal closed system ascent of LP magmas (melt composition data Métrich et al., 2010) within their storage zone (300–190 MPa pressure range), and upon shallow emplacement (down to 100 MPa). Redox conditions along the decompression path were fixed by the Fe^{2+}/Fe^{3+} buffer, for which we adopted the value of 3.4. This choice is based on XANES determinations on a hydrous ($H_2O = 2.9$ wt.%) LP magma melt inclusion (Bonnin-Mosbah et al., 2001), but is also consistent with the olivine-liquid iron and magnesium partition observed in a large set of Stromboli MIs (Bertagnini et al., 2003). The resulting $logfO_2$ conditions range from 0.07 to 0.82 NNO (NNO is the Nickel–Nickel Oxide buffer). Note that while MI compositions can be taken as good proxies for total (exsolved + dissolved) water and sulphur contents (then evaluated as $H2O^{TOT}$: 3.4 wt.%; S^{TOT}: 0.16 wt.%, respectively), LP magmas were probably already saturated with a CO_2-rich gas phase when the most primitive MIs formed. If such, the highest measured dissolved CO_2 content (~0.2 wt.%; see Fig. 7a) in MIs would significantly underestimate $CO2^{TOT}$. Four separate LP runs (with different $CO2^{TOT}$ contents; these should be viewed as CO_2 concentrations in the magma, i.e., in the melt plus gas suspension) were thus carried out. As for HP runs, we considered a shoshonitic melt with total CO_2, H_2O, and S contents of 0.04, 1.2 and 0.1 wt.%, respectively (as from representative compositions of MIs in olivines from erupted HP products; Métrich et al., 2010). The recurrent observation of a sulphide immiscible liquid phase in MIs suggests that the HP magma is potentially in a more reducing redox state than the LP magma; we therefore performed model runs at both NNO at NNO-1 redox conditions. For both LP and HP runs, melt composition data are from Métrich et al. (2010).

Run ID	T (K)	P (MPa)	Degassing mode	Redox[a] (ΔNNO)	H_2O^{TOT} wt.%	CO_2^{TOT} wt.%	S^{TOT} wt.%	Melt composition
LP runs								
1	1423	Decompression from 300 to 100	Closed system	0.07 ÷ 0.82 ($Fe^{3+}/Fe_{tot} = 0.24$)	3.4	0.2	0.16	SiO_2 TiO_2 Al_2O_3 FeO_{tot} 51.6 0.9 16.2 8.42 MgO CaO Na_2O K_2O 6.64 10.6 2.5 1.9
2	1423	Decompression from 300 to 100	Closed system	0.07 ÷ 0.82 ($Fe^{3+}/Fe_{tot} = 0.24$)	3.4	2	0.16	MgO CaO Na_2O K_2O 6.64 10.6 2.5 1.9
3	1423	Decompression from 300 to 100	Closed system	0.07 ÷ 0.82 ($Fe^{3+}/Fe_{tot} = 0.24$)	3.4	5	0.16	MgO CaO Na_2O K_2O 6.64 10.6 2.5 1.9
4	1423	Decompression from 300 to 100	Closed system	0.07 ÷ 0.82 ($Fe^{3+}/Fe_{tot} = 0.24$)	3.4	20	0.16	MgO CaO Na_2O K_2O 6.64 10.6 2.5 1.9
HP runs[b]								
5	1383	Decompression from 100 to 0.1	Closed system from 100 to 50 MPa; open system from 50 to 0.1	−1	1.2	0.04	0.1	SiO_2 TiO_2 Al_2O_3 FeO_{tot} 52.6 1.7 15.6 11.27 MgO CaO Na_2O K_2O 3.27 7.41 3.7 4.2
6	1383	Decompression from 100 to 0.1	Closed system from 100 to 50 MPa; open system from 50 to 0.1	0	1.2	0.04	0.1	MgO CaO Na_2O K_2O 3.27 7.41 3.7 4.2

[a] NNO refers to the nickel–nickel oxide buffer.
[b] A note of caution should be spent on the application of the H_2O–CO_2 model (Papale et al., 2006) on shoshonitic composition. This model is in fact highly sensitive on Fe^{2+}/Fe^{3+} partition, hence fO_2. Only few data with known experimental oxygen fugacity were available for model calibration, then limiting the accuracy of predictions on those iron-rich melt compositions for which CO_2 solubility and H_2O–CO_2 saturation data were missing, such as shoshonites. Standard deviations of model binary interaction terms show maximum values for iron oxides, because they encompass all uncertainties on fO_2 conditions within the calibration dataset (Papale et al., 2006). As such, the high range of entrapment pressures for HP MIs reported here, estimated at 100 MPa, can be decreased down to 80 MPa when adopting NNO-1 redox conditions.

the CO_2-rich gas bubbles may be thought to be sourced by the deep (7–11 km deep) LP magma storage zone; though partial gas-melt re-equilibration at shallower depths (and particularly upon gas bubble accumulation within — before leakage from — the intermediate 2–4 km deep magma ponding zone) cannot be ruled out.

Secondly, there is supporting evidence at Stromboli for that continuous magma convection takes place within the shallow (<1 km) dyke system (Harris and Stevenson, 1997). This degassing-driven process (Shinohara, 2008) occurs in response to the sinking of the degassed (non-erupted) HP magma back into the conduit, and its replacement with ascending vesicular (and thus less-dense) magma blobs. The shallow convective overturning of the HP magma obviously gives rise to a second source of volatiles: degassing of dissolved volatiles in the ascending HP magma will produce gas bubbles which pressure-dependent compositional evolution is best described by curves 5 and 6 in Fig. 8. According to the figure, the composition of this shallow gas contribution will be dependent on the final depth (pressure) of magma ascent in the upper conduits; assuming near-surface magma ascent and gas separation, the HP gas would correspond to the modelled gas composition calculated at 0.1 MPa in HP runs 5–6.

In the light of this dual gas origin at Stromboli, we therefore consider a mechanism in which surface gas discharges are produced in the following manner. CO_2-rich gas bubbles are persistently supplied to the shallow plumbing system by degassing (and gas-melt separation) in the LP magma storage zone. We take the calculated magmatic gas composition for the LP run 2 at the reservoir pressure of ~210 MPa as representative of this rising CO_2-rich vapour phase. We then make the guess that the rising gas bubbles mix, upon their ascent, with gases released by degassing of dissolved volatiles in the shallow HP magma. Taking the modelled gas composition at 0.1 MPa (from HP runs 5 and/or 6) as representative of this shallow gas contribution, we obtain the mixing lines drawn in Figs. 5 and 8. Fig. 5, in particular, demonstrates a fair agreement between the model mixing lines and the compositional trends shown by our volcanic gas measurements. From this, we therefore conclude that a time-variable but persistent supply of deeply derived CO_2-rich gas bubbles, mixing in variable proportions with gases derived from the shallow HP reservoir, is a sound mechanism to generate Stromboli's surface gas discharges; and we calculate that LP gas contributions to the mixture of 6–40% (~20% as time average) well account for the temporal range of our gas compositions. If this interpretation is correct, an increase in CO_2 proportions (relative to H_2O and SO_2) in gas discharges at Stromboli should be taken as sign of increasing deep gas supply relative to the shallow gas contribution, and thus possibly as precursory sign of LP magma degassing prior to paroxysm (Aiuppa et al., 2009).

6. Conclusions

The MultiGAS volcanic gas observations presented here show that, in spite of the relatively uniform activity and petrology of erupted solid materials, Stromboli shares with other basaltic volcanoes an exceptional variability in gas compositions. The mechanisms controlling such time-changing nature of Stromboli's gas emissions have been explored by combining gas measurements with the MI record of volatile abundance in magmas, and by contrasting natural compositions with model results derived with an equilibrium saturation code. From this, we propose that the compositional features of Stromboli's quiescent and syn-explosive gas emissions result from the mixing of gases persistently sourced by (i) degassing of dissolved volatiles in the porphyric magma filling the

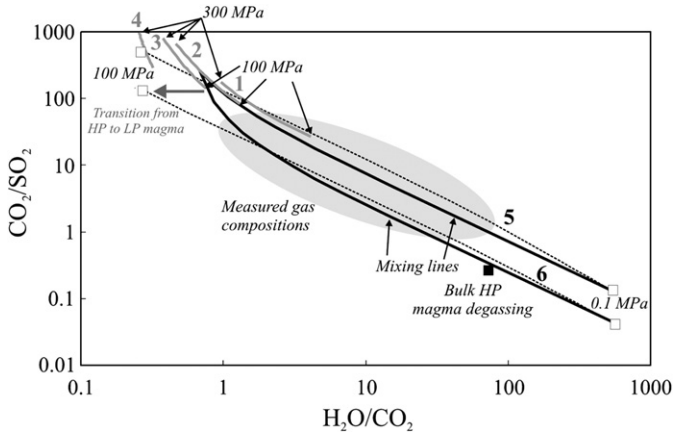

Fig. 8. Gas-phase model results summarised in a H_2O/CO_2 vs. CO_2/SO_2 scatter plot. The grey solid lines show modelled gas compositions in LP runs 1–4 over the 300–100 MPa pressure range. Black dashed lines illustrate model results of the evolution of the magmatic gas phase formed by decompression (100–0.1 MPa pressure range) of the HP magma (HP runs 5–6). The curves labelled "Mixing lines" simulate mixing of CO_2-rich gas bubbles in equilibrium with the LP magma at 210 MPa (LP run 2) with the gas phase produced by degassing of dissolved volatiles in the HP magma at 0.1 MPa (runs 5–6). The dashed area marks the field of measured gas compositions. The black square symbol labelled "bulk HP magma degassing" represents the hypothetical composition of the gas phase produced via closed system (bulk) degassing of the HP magma upon decompression from 100 to 0.1 MPa. Clearly, this is CO_2-poorer than our observed gas compositions. A zoom on the comparison between measured and modelled gas compositions is given in Fig. 5.

upper (<1 km) dyke-conduit system; and (ii) CO_2-rich gas bubbles, originated at depth (at depths >4 km, or P>100 MPa) in the plumbing system. Both gas contributions are persistent and concur to determine gas discharges, and the temporal fluctuations in their source strengths (which may reflect the simultaneous action of a number of factor, such as changes in magma convection rate or gas content, and/or a structural/tectonic control on the rate of gas bubble supply from depth) are at the base of the striking variability in Stromboli's gas emissions; with phases of increasing supply of deep-rising gas bubbles reflecting into CO_2-enriched signatures of surface emissions, potentially being precursory to large scale deeply-sourced paroxysms.

The proposed mixing mechanism is constrained by independent petrologic and model data, and it is geologically straightforward since it only requires a persistent but time-modulated source of deep gas bubbles; this however does not exclude that additional control mechanisms on volcanic gas composition might be at work. We conclude however that, since magma fluxing by a free CO_2-rich vapour phase is a recurrent process, the proposed degassing mechanism is probably a key to interpret volcanic gas observations at many basaltic volcanoes.

Acknowledgements

This manuscript has benefited from the valuable comments of two anonymous reviewers and the editor (R.W. Carlson). S. Gurrieri, G. Giudice and the INGV staff are acknowledged.

References

Aiuppa, A., Moretti, R., Federico, C., Giudice, G., Gurrieri, S., Liuzzo, M., Papale, P., Shinohara, H., Valenza, M., 2007. Forecasting Etna eruption by real time evaluation of volcanic gas composition. Geology 35 (12), 1115–1118 doi:10.1130/G24149A.

Aiuppa, A., Federico, C., Giudice, G., Giuffrida, G., Guida, R., Gurrieri, S., Liuzzo, M., Moretti, R., Papale, P., 2009. The 2007 eruption of Stromboli volcano: insights from real-time measurements of the volcanic gas plume CO_2/SO_2 ratio. J. Volcanol. Geoth. Res. 182, 221–230.

Allard, P., 2010. A CO_2-rich gas trigger of explosive paroxysms at Stromboli basaltic volcano, Italy. J. Volcanol. Geoth. Res. 189, 363–374.

Allard, P., Burton, M., Muré, F., 2004. Spectroscopic evidence for a lava fountain driven by previously accumulated magmatic gas. Nature 433, 407–410 doi:10.1038/nature03246.

Allard, P., Aiuppa, A., Burton, M., Caltabiano, T., Federico, C., Salerno, G., La Spina, A., 2008. Crater gas emissions and the magma feeding system of Stromboli volcano. In: Calvari, S., Inguaggiato, S., Puglisi, G., Ripepe, M., Rosi, M. (Eds.), Learning from Stromboli: AGU Geophysics Monograph Series, 182, pp. 65–80. Washington DC.

Bertagnini, A., Métrich, N., Landi, P., Rosi, M., 2003. Stromboli an open window on the deep feeding system of a steady state volcano. J. Geophys. Res. 108 (B7), 2336 doi:10.1029/2002JB002146.

Bertagnini, A., Métrich, N., Francalanci, L., Landi, P., Tommasini, S., Conticelli, S., 2008. Volcanology and magma geochemistry of the present-day activity: constraints on the feeding system. In: Calvari, S., Inguaggiato, S., Puglisi, G., Ripepe, M., Rosi, M. (Eds.), Learning from Stromboli: AGU Geophysics Monograph Series, 182, pp. 19–38. Washington DC.

Blundy, J., Cashman, K., 2008. Petrologic reconstruction of magmatic system variables and processes. Rev. Mineralog. Geochem. 69, 179–239.

Bonaccorso, A., Gambino, S., Guglielmino, F., Mattia, M., Puglisi, G., Boschi, E., 2008. Stromboli 2007 eruption: deflation modeling to infer shallow-intermediate plumbing system. Geophys. Res. Lett. 35, L06311 doi:10.1029/2007GL032921.

Bonnin-Mosbah, M., Simionovici, A.S., Métrich, N., Duraud, J.P., Massare, D., Dillmann, P., 2001. Iron oxidation states in silicate glass fragments and glass inclusions with a XANES micro-probe. J. Non-Cryst. Solids 288, 103–113.

Burton, M.R., Oppenheimer, C., Horrocks, L.A., Francis, P.W., 2000. Remote sensing of CO_2 and H_2O emission rates from Masaya volcano, Nicaragua. Geology 28 (10), 915–918.

Burton, M.R., Mader, H.M., Polacci, M., 2007a. The role of gas percolation in quiescent degassing of persistently active basaltic volcanoes. Earth Planet. Sci. Lett. 264, 46–60.

Burton, M.R., Allard, P., Muré, F., La Spina, A., 2007b. Magmatic gas composition reveals the source depth of slug-driven strombolian explosive activity. Science 37, 227–230.

Collins, S.J., Pyle, D.M., Maclennan, J., 2009. Melt inclusions track pre-eruption storage and dehydration of magmas at Etna. Geology 37, 571–574 doi:10.1130/G30040A.1.

Di Carlo, I., Pichavant, M., Rotolo, S., Scaillet, B., 2006. Experimental crystallization of a high-K arc basalt: the Golden Pumice, Stromboli Volcano (Italy). J. Petrol. 1–27 doi:10.1093/petrology/egl011.

Di Roberto, A., Bertagnini, A., Pompilio, M., Gamberi, F., Marani, M.P., Rosi, M., 2008. Newly discovered submarine flank eruption at Stromboli volcano (Aeolian Islands, Italy). Geophys. Res. Lett. 35, L16310 doi:10.1029/2008GL034824.

Edmonds, M., 2008. New geochemical insights into volcanic degassing. Philos. Trans. R. Soc. A 366, 4559–4579.

Edmonds, M., Gerlach, T.M., 2007. Vapor segregation and loss in basaltic melts. Geology 35, 751–754 doi:10.1130/G2346A.1.

Harris, A., Ripepe, M., 2007. Temperature and dynamics of degassing at Stromboli. J. Geophys. Res. 112, B03205 doi:10.1029/2006JB004393.

Harris, A.J.L., Stevenson, D.S., 1997. Magma budgets and steady-state activity of Vulcano and Stromboli volcanoes. Geophys. Res. Lett. 24, 1043–1046.

Johnson, E.R., Wallace, P.J., Cashman, K.V., Delgado Granados, H., Kent, A.J.R., 2008. Magmatic volatile contents and degassing-induced crystallization at Volcán Jorullo, Mexico: implications for melt evolution and the plumbing systems of monogenetic volcanoes. Earth Planet. Sci. Lett. 269, 478–487.

Landi, P., Corsaro, R.A., Francalanci, L., Civetta, L., Miraglia, L., Pompilio, M., Tesoro, R., 2009. Magma dynamics during the 2007 Stromboli eruption (Aeolian islands, Italy): mineralogical, geochemical and isotopic data. J. Volcanol. Geoth. Res. 182, 255–268 doi:10.1016/j.jvolgeores.2008.11.010.

Métrich, N., Wallace, P., 2008. Volatile abundances in basaltic magmas and their degassing paths tracked by melt inclusions. In: Putirka, K., Tepley, F. (Eds.), Minerals, Inclusions and Volcanic Processes: Reviews in Mineralogy and Geochemistry, 69, pp. 363–402.

Métrich, N., Bertagnini, A., Landi, P., Rosi, M., 2001. Crystallisation driven by decompression and water loss at Stromboli volcano (Aeolian Islands). J. Petrol. 42, 1471–1490.

Métrich, N., Bertagnini, A., Landi, P., Rosi, M., Belhadj, O., 2005. Triggering mechanism at the origin of paroxysms at Stromboli (Aeolian archipelago, Italy): the 5 April 2003 eruption. Geophys. Res. Lett. 32, L103056 doi:10.1029/2004GL022257.

Métrich, N., Bertagnini, A., Di Muro, A., 2010. Conditions of magma storage, degassing and ascent at Stromboli: new insights into the volcano plumbing system with inferences on the eruptive dynamics, J. Petrol. 51, 603–626. doi: 10.1093-petrology-egp083.

Moretti, R., Papale, P., 2004. On the oxidation state and volatile behaviour in multicomponent gas-melt equilibria. Chem. Geol. 213, 265–280.

Papale, P., Moretti, R., Barbato, D., 2006. The compositional dependence of the saturation surface of $H_2O + CO_2$ fluids in silicate melts. Chem. Geol. 29, 78–95.

Pichavant, M., Di Carlo, I., Le Gac, Y., Rotolo, S.G., Scaillet, B., 2009. Experimental constraints on the deep magma feeding system at Stromboli volcano, Italy. J. Petrol. 50, 601–624 doi:10.1093/petrology/egp014.

Polacci, M., Baker, D.R., Mancini, L., Favretto, S., Hill, R.J., 2009. Vesiculation in magmas from Stromboli and implications for normal Strombolian activity and paroxysmal explosions in basaltic systems. J. Geophys. Res. 114 art. no. B01206.

Ripepe, M., Delle Donne, D., Harris, A., Marchetti, E., Ulivieri, G., 2008. Dynamics of Stromboli activity. In: Calvari, S., Inguaggiato, S., Puglisi, G., Ripepe, M., Rosi, M. (Eds.), Learning from Stromboli: AGU Geophysics Monograph Series, 182, pp. 39–48. Washington DC.

Rosi, M., Bertagnini, A., Landi, P., 2000. Onset of the persistent activity at Stromboli volcano (Italy). Bull. Volcanol. 62, 294–300.

Rust, A.C., Cashman, K.V., Wallace, P.J., 2004. Magma degassing buffered by vapour flow through brecciated conduit margins. Geology 32 (4), 349–352 doi:10.1130/G20388.1.

Sawyer, G.M., Carn, S.A., Tsanev, V.I., Oppenheimer, C., Burton, M., 2008. Investigation into magma degassing at Nyiragongo volcano, Democratic Republic of Congo. Geochem. Geophys. Geosyst. 9, Q02017 doi:10.1029/2007GC001829.

Shinohara, H., 2008. Excess degassing from volcanoes and its role on eruptive and intrusive activity. Rev. Geophys. 46 doi:10.1029/2007RG000244 RG4005.

Shinohara, H., Aiuppa, A., Giudice, G., Gurrieri, S., Liuzzo, M., 2008. Variation of H_2O/CO_2 and CO_2/SO_2 ratios of volcanic gases discharged by continuous degassing of Mt. Etna Volcano, Italy. J. Geophys. Res. doi:10.1029/2007JB005185

Spilliaert, N., Allard, P., Métrich, N., Sobolev, A., 2006. Melt inclusion record of the conditions of ascent, degassing and extrusion of volatile-rich alkali basalt during the powerful 2002 flank eruption of Mount Etna (Italy). J. Geophys. Res. 111, B04203 doi:10.1029/2005/JB003934.